# First-in-Human Human Epidermal Growth Factor Receptor 2–Targeted Imaging Using [89]Zr-Pertuzumab PET/CT: Dosimetry and Clinical Application in Patients with Breast Cancer

Gary A. Ulaner[1,2], Serge K. Lyashchenko[1,2], Christopher Riedl[1,2], Shutian Ruan[3], Pat B. Zanzonico[3], Diana Lake[4,5], Komal Jhaveri[4,5], Brian Zeglis[6], Jason S. Lewis[1,2,7], and Joseph A. O'Donoghue[3]

[1]Department of Radiology, Memorial Sloan Kettering Cancer Center, New York, New York; [2]Department of Radiology, Weill Cornell Medical College, New York, New York; [3]Department of Medical Physics, Memorial Sloan Kettering Cancer Center, New York, New York; [4]Department of Medicine, Memorial Sloan Kettering Cancer Center, New York, New York; [5]Department of Medicine, Weill Cornell Medical College, New York, New York; [6]Department of Chemistry, Hunter College, New York, New York; and [7]Program in Molecular Pharmacology, Memorial Sloan Kettering Cancer Center, New York, New York

In what we believe to be a first-in-human study, we evaluated the safety and dosimetry of [89]Zr-pertuzumab PET/CT for human epidermal growth factor receptor 2 (HER2)–targeted imaging in patients with HER2-positive breast cancer. **Methods:** Patients with HER2-positive breast cancer and evidence of distant metastases were enrolled in an institutional review board–approved prospective clinical trial. Pertuzumab was conjugated with deferoxamine and radiolabeled with [89]Zr. Patients underwent PET/CT with 74 MBq of [89]Zr-pertuzumab in a total antibody mass of 20–50 mg of pertuzumab. PET/CT, whole-body probe counts, and blood drawing were performed over 8 d to assess pharmacokinetics, biodistribution, and dosimetry. PET/CT images were evaluated for the ability to visualize HER2-positive metastases. **Results:** Six patients with HER2-positive metastatic breast cancer were enrolled and administered [89]Zr-pertuzumab. No toxicities occurred. Dosimetry estimates from OLINDA demonstrated that the organs receiving the highest doses (mean ± SD) were the liver (1.75 ± 0.21 mGy/MBq), the kidneys (1.27 ± 0.28 mGy/MBq), and the heart wall (1.22 ± 0.16 mGy/MBq), with an average effective dose of 0.54 ± 0.07 mSv/MBq. PET/CT demonstrated optimal imaging 5–8 d after administration. [89]Zr-pertuzumab was able to image multiple sites of malignancy and suggested that they were HER2-positive. In 2 patients with both known HER2-positive and HER2-negative primary breast cancers and brain metastases, [89]Zr-pertuzumab PET/CT suggested that the brain metastases were HER2-positive. In 1 of the 2 patients, subsequent resection of a brain metastasis proved HER2-positive disease, confirming that the [89]Zr-pertuzumab avidity was a true-positive result for HER2-positive malignancy. **Conclusion:** This first-in-human study demonstrated safety, dosimetry, biodistribution, and successful HER2-targeted imaging with [89]Zr-pertuzumab PET/CT. Potential clinical applications include assessment of the HER2 status of lesions that may not be accessible to biopsy and assessment of HER2 heterogeneity.

Human epidermal growth factor receptor 2 (HER2) is a critical biomarker in breast cancer, and its expression directly influences treatment. Approximately 20% of invasive ductal breast malignancies are classified as HER2-positive as a result of *ERBB2* gene amplification or the subsequent overexpression of the HER2 protein on the surface of tumor cells (*1*). Patients with HER2-positive breast cancer receive specific therapies that are targeted to HER2 and that reduce the risk of death, whereas patients with HER2-negative breast cancer do not receive them (*2,3*). This situation has resulted in considerable interest in HER2-targeted imaging (*4*). Recent work has demonstrated the ability to detect HER2-positive metastases in patients with HER2-negative primary breast tumors by HER2-targeted imaging confirmed with immunohistochemistry (IHC) (*5,6*) and molecular analyses (*7*). Thus, the ability to perform noninvasive, whole-body, HER2-targeted imaging may be valuable in the detection of otherwise unsuspected HER2-positive malignancies and may help direct appropriate HER2-targeted therapy.

Although there have been successes in HER2-targeted imaging with [89]Zr-trastuzumab, there have also been examples of nonspecific visualization of malignancies that are HER2-negative on pathology (*5,6*). More specific HER2-targeted agents may be needed for clinical translation of HER2-targeted imaging agents. Pertuzumab is a newer humanized monoclonal antibody that binds to the HER2 receptor at a site distinct from that bound to by trastuzumab and appears to be more efficient than trastuzumab (*8*). In vitro and in vivo models have demonstrated successful [89]Zr-pertuzumab targeting to HER2-positive malignancies and, notably, have demonstrated increased affinity for HER2 in the presence of trastuzumab (*9*)—as may be the case in patients who have HER2-positive malignancies and are receiving trastuzumab. Here we present the

results of what we believe to be a first-in-human study of HER2-targeted imaging with [89]Zr-pertuzumab PET/CT, performed to document the safety, dosimetry, and potential clinical utility of this HER2-targeted imaging agent.

## MATERIALS AND METHODS

### Patients

This study was performed under a single-center prospective Memorial Sloan Kettering Cancer Center Institutional Review Board–approved protocol (ClinicalTrials.gov identifier NCT03109977). All patients provided written informed consent. Patients with pathologically proven HER2-positive metastatic breast cancer were identified as potential candidates. HER2 positivity was defined according to American Society of Clinical Oncology guidelines (10), including 3+ HER2 IHC or 2+ HER2 IHC with HER2 amplification on fluorescence in situ hybridization (FISH) of 2.0 or more; 0 or 1+ IHC or 2+ IHC with HER2 amplification on FISH of less than 2.0 was considered HER2-negative. The 4 inclusion criteria were biopsy-proven, HER2-positive malignancy; foci of malignancy on imaging within 60 d of enrollment; women who were 21 years old or older; and Eastern Cooperative Oncology Group performance score of 0–2 (11). The 3 exclusion criteria were life expectancy of less than 3 mo; pregnancy or lactation; and inability to undergo PET/CT scanning because of weight limits. A biopsy demonstrating HER2-positive malignancy was required for inclusion. The HER2-positive biopsy was allowed at any time during the patient's disease course and could be from the primary breast malignancy or a site of metastatic disease. Patients were allowed to be on HER2-directed therapy. Sites of known malignancy were determined by medical imaging, including CT, MRI, and ^{18}F-FDG PET/CT, within 60 d of protocol enrollment. As part of the inclusion criteria, the primary malignancy and at least 1 site of distant metastasis had to be pathologically proven.

### [89]Zr-Pertuzumab Preparation

[89]Zr-deferoxamine-pertuzumab was manufactured at the Memorial Sloan Kettering Radiochemistry and Molecular Imaging Probes Core Facility in compliance with the requirements specified in the Chemistry, Manufacturing, and Controls section of a U.S. Food and Drug Administration–acknowledged Investigational New Drug application (134411). The preparation process involved conjugating clinical-grade pertuzumab (Perjeta; Genentech) with a bifunctional chelator, p-SCN-Bn-deferoxamine (Macrocyclics), and then radiolabeling with [89]Zr, a radiometal positron emitter with a 78.4-h radioactive half-life. The conjugation and radiolabeling were performed using previously described methodology (12). Radiolabeling with [89]Zr was chosen because of the favorable properties of this metalloradionuclide, such as radioactive half-life (which is long enough to allow for the imaging of radiolabeled antibodies after localization at the target site has occurred) as well as mild radiolabeling conditions (at an ambient temperature in 1 M ammonium acetate buffer; pH 7); these properties help to preserve pertuzumab protein integrity and immunoreactivity during the radiolabeling process (13,14).

The [89]Zr-deferoxamine-pertuzumab final drug product batches underwent quality control testing before batch release for patient administration, to ensure conformance to the following acceptance specifications: radiochemical purity, as determined by radio–thin-layer chromatography and size-exclusion high-performance liquid chromatography; radioimmunoreactivity, as determined using a live antigen–expressing cell binding assay; endotoxin content, as measured using a portable test system supplied by Charles River Laboratories; sterilizing filter integrity, as measured by the bubble point method; pH, as measured using pH strips; appearance as a clear and particle-free solution, as determined by visual inspection check; and radionuclidic identity verification, as measured by radioactive γ-spectroscopy. Sterility testing using the direct medium inoculation method was performed after release.

### [89]Zr-Pertuzumab Administration

An intravenous line was established and flushed with 5% human serum albumin solution. Nonradiolabeled pertuzumab (18 or 48 mg) was then intravenously administered over 5 min. Cold pertuzumab was administered to help reduce nonspecific uptake of the subsequently administered radiolabeled pertuzumab. Next, 74 MBq ± 10% of [89]Zr-pertuzumab was intravenously administered in a mass of approximately 2 mg to bring the total pertuzumab antibody mass for each patient to 20 or 50 mg. The first 2 patients were administered 50 mg; the antibody mass was reduced to 20 mg for the next 2 patients. Visual analysis suggested that 50 mg of total antibody mass produced lower background uptake; thus, the total antibody mass was increased to 50 mg for the last 2 patients. Patients were monitored for side effects on the day of and on the day after [89]Zr-pertuzumab administration.

### [89]Zr-Pertuzumab PET/CT and Image Analysis

Up to 4 whole-body PET/CT scans were obtained for each patient on days 1, 2–4, 5 or 6, and 7 or 8 after the administration (day 0) of [89]Zr-pertuzumab. The days of imaging were preselected before the protocol was opened to allow both comprehensive multiday imaging and flexibility of scheduling, particularly over the weekend.

Patients were imaged from the skull apex to the midthigh on a dedicated research PET/CT scanner (GE Discovery 710) in 3-dimensional mode with emission time per bed position extending from 4 min (day 1) to 8 min (day 7 or 8). Low-dose CT scans were acquired with an x-ray tube current of 80 mA. PET/CT images were reconstructed with attenuation, scatter, and other standard corrections applied and with iterative reconstruction. [89]Zr-pertuzumab PET/CT scans were interpreted by a nuclear radiologist with experience in HER2-targeted imaging and knowledge of the patient's medical history and prior imaging. Nonphysiologic radiotracer uptake was considered suggestive of HER2-positive malignancy. Volumes of interest were drawn on PET/CT images over normal liver, kidney, spleen, and lung using a dedicated workstation (Hermes Medical Solutions). Normal tissue uptake was quantified as the mean SUV adjusted to lean body mass ($SUV_{LBM}$).

### Whole-Body and Serum Clearance Measurements

Whole-body clearance was determined by serial measurements of counting rates using a 12.7-cm-thick NaI(Tl) scintillation detector at a fixed 3 m from the patient. Background-corrected geometric mean counts were obtained after infusion before and after voiding and, subsequently, at the times of the PET scans ($n = 6$). Counting rates were normalized to the immediate postinfusion value (taken as 100%) to yield relative retained activities (as percentages).

Multiple blood samples were obtained at approximately 15 min, 30 min, 1–2 h after injection and, subsequently, at the time of each PET scan ($n = 7$). Counts in aliquots of serum were obtained using a γ-well-type detector (Wallac Wizard 1480 γ-counter; Perkin Elmer), and measured activity concentrations were converted to percentage injected activity/L.

A monoexponential function was fitted to the whole-body probe data and a biexponential function was fitted to the serum activity concentration data using SAAM software (15). Areas under the curve (AUCs) and corresponding residence times were derived by analytic integration.

### Normal Tissue Dosimetry

Normal tissue dose estimates were derived as described previously (16,17). In brief, image-derived $SUV_{LBM}$ was converted to activity concentration per unit of mass (kBq/g), and AUCs were estimated by trapezoidal integration. Whole-organ AUCs were estimated by multiplying the activity concentration AUCs by the projected organ

## TABLE 1
### Characteristics of 6 Women with IDC

| Patient | Age (y) | Sites of known malignancy at time of $^{89}$Zr-pertuzumab administration | Days after $^{89}$Zr-pertuzumab administration on which PET/CT imaging was done | Sites of demonstrably $^{89}$Zr-pertuzumab–avid disease |
|---------|---------|---------------------------------------|------------------------------|-----------------------------|
| 1 | 46 | Brain | 1, 2, 6, 8 | Brain |
| 2 | 68 | Nodal | 1, 2, 5, 7 | Nodal |
| 3 | 58 | Breast, nodal | 1, 2, 6, 7 | Breast, nodal |
| 4 | 69 | Liver, bone, chest wall | 1, 4, 5, 8 | Chest wall |
| 5 | 38 | Brain, lung, nodal, liver | 1, 2, 5 | Brain, lung, nodal |
| 6 | 42 | Nodal | 1, 4, 5, 7 | None |

mass. Residence times were derived by dividing whole-organ AUCs by the administered activity. Corresponding values for heart contents and red marrow were estimated from the serum AUCs (*18*). The residence time for the remainder of the body was derived by subtracting all individually estimated residence times from the whole-body residence time. Thereafter, absorbed radiation doses to individual organs were calculated using the OLINDA/EXM software application (*19*).

### Comparison of $^{89}$Zr-Pertuzumab Dosimetry with $^{89}$Zr-Trastuzumab Dosimetry

Tissue dosimetry and total-body dosimetry were compared for the newly calculated values for $^{89}$Zr-pertuzumab and for published values for $^{89}$Zr-trastuzumab.

### Statistics

Kinetic parameters and absorbed dose estimates were calculated for each patient on an individual basis. Subsequently, these data were summarized using descriptive statistics.

## RESULTS

### Patient Characteristics

Between April and June 2017, 6 patients, all women with biopsy-proven HER2-positive malignancies from invasive ductal breast cancer (IDC), completed the study protocol. All patients underwent imaging on days 1, 2–4, 5 or 6, or 7 or 8 as prescribed in the prospective protocol. Patient characteristics are summarized in Table 1.

### Sites of Known Malignancy at Time of Protocol Enrollment

Sites of known malignancy were determined from medical imaging within 60 d of protocol enrollment. Known nodal disease was present in 4 patients, brain malignancies were present in 2, hepatic malignancies were present in 2, and malignancies involving the breast, bone, chest wall, and lung each were present in 1 patient. Sites of known malignancy are summarized in Table 1.

### Adverse Events

All 6 patients underwent $^{89}$Zr-pertuzumab administration. Patients were monitored for 2 h after tracer injection and evaluated on the following day when they returned for PET/CT imaging, and no side effects were observed or reported. Vital signs were recorded before and after tracer administration, and there were no changes with clinical significance. Safety data were reviewed and approved by the U.S. Food and Drug Administration as part of the Investigational New Drug application.

### Pharmacokinetics

Whole-body clearance and serum clearance conformed to mono- and biexponential kinetics, respectively. Summed biologic clearance curves are shown in Figure 1. Summary statistics for the clearance parameters are provided in Table 2.

### Biodistribution and Normal Tissue Dose Estimates

$^{89}$Zr-pertuzumab uptake was observed in the blood pool, liver, kidney, and spleen. There was little measureable change in whole-body activity after the first void (98% $\pm$ 1.8% [mean $\pm$ SD] of the prevoid measurement). The urinary bladder was not visualized on any PET/CT scan. Bowel excretion was visualized in 2 patients on day 1 and 2 scans. Uptake in the liver and kidneys, in terms of $SUV_{LBM}$, was relatively constant over the duration of imaging, whereas blood-pool and spleen uptake decreased over time. These sites of tracer visualization were considered physiologic. Absorbed dose estimates for normal tissues are provided in Table 3. The organs receiving the highest doses were the liver (1.75 $\pm$ 0.21 mGy/MBq), kidneys (1.27 $\pm$ 0.28 mGy/MBq), and heart wall (1.22 $\pm$ 0.16 mGy/MBq), with an average effective dose of 0.54 $\pm$ 0.07 mSv/MBq.

### Comparison of $^{89}$Zr-Pertuzumab Dosimetry with $^{89}$Zr-Trastuzumab Dosimetry

The mean effective dose of $^{89}$Zr-pertuzumab was 0.54 mSv/MBq. Figure 2 shows the comparative absorbed dose estimates for both antibodies.
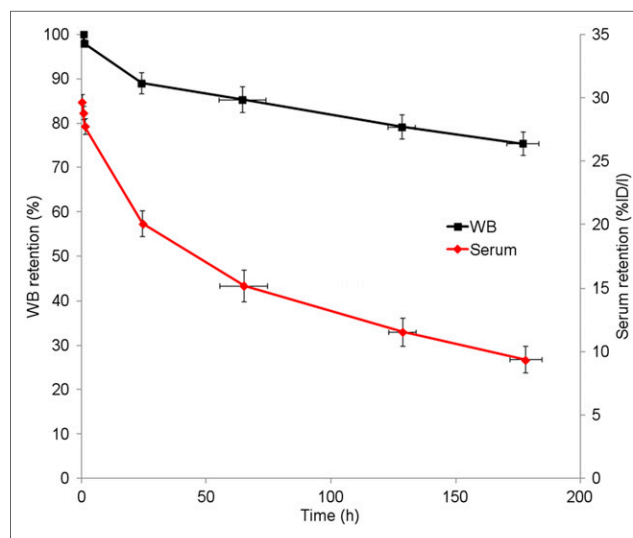


**FIGURE 1.** Summed whole-body (WB) and serum biologic clearance data for $^{89}$Zr-pertuzumab in 6 patients. Error bars indicate SE of mean. %ID/l = percentage injected dose/L.

TABLE 2
Summary Statistics for Whole-Body and Serum Clearance

| Measurement | Whole body | | Serum | | | | | |
|---|---|---|---|---|---|---|---|---|
| | $t_{1/2}$ eff | $t_{1/2}$ bio | A1 (%/L) | $t_{1/2}$ α eff | $t_{1/2}$ α bio | A2 (%/L) | $t_{1/2}$ β eff | $t_{1/2}$ β bio |
| Mean | 67.7 | 521 | 12.6 | 12.1 | 15.5 | 17.3 | 59.3 | 201 |
| SD | 2.3 | 145 | 5.3 | 7.8 | 11.5 | 5.0 | 10.3 | 72 |
| Median | 66.9 | 456 | 13.0 | 9.7 | 11.2 | 16.3 | 55.5 | 176 |
| Minimum | 65.2 | 387 | 5.6 | 3.1 | 3.3 | 11.7 | 50.4 | 141 |
| Maximum | 70.8 | 730 | 18.8 | 22.1 | 30.8 | 23.3 | 78.4 | 322 |

eff = effective half-life; bio = biologic half-life; A1 = partition coefficient for fast component of serum clearance; α = half-time for fast component of serum clearance; A2 = partition coefficient for slow component of serum clearance; β = half-time for slow component of serum clearance.

Whole-body clearance was monoexponential. Serum clearance was biexponential and conformed to the following equation: A1exp(−a1t) + A2exp(−a2t). A1 and A2 are partition coefficients, and respective $t_{1/2}$ values correspond to ln(2)/a. All half-lives are in hours.

## Imaging of Lesions with 89Zr-Pertuzumab PET/CT

Patient 1 had 2 known primary breast malignancies, a right breast estrogen receptor (ER)–positive, progesterone receptor (PR)–positive, and HER2-positive (HER2 IHC 3+) IDC diagnosed in 2014 and an ER-positive, PR-positive, and HER2-negative (HER2 IHC 0) IDC diagnosed in 2015. She had received HER2-directed

TABLE 3
Absorbed Dose Estimates for Normal Tissues

| Target organs or measurement | Absorbed dose estimates (mGy/MBq) | | | | |
|---|---|---|---|---|---|
| | Mean | SD | Median | Minimum | Maximum |
| Adrenal glands | 0.64 | 0.17 | 0.69 | 0.31 | 0.80 |
| Brain | 0.25 | 0.06 | 0.24 | 0.15 | 0.33 |
| Breasts | 0.33 | 0.08 | 0.35 | 0.18 | 0.41 |
| Gallbladder wall | 0.69 | 0.18 | 0.72 | 0.34 | 0.83 |
| Lower large intestinal wall | 0.42 | 0.06 | 0.40 | 0.36 | 0.52 |
| Small intestine | 0.39 | 0.09 | 0.40 | 0.22 | 0.51 |
| Stomach wall | 0.46 | 0.12 | 0.49 | 0.23 | 0.59 |
| Upper large intestinal wall | 0.46 | 0.09 | 0.47 | 0.30 | 0.57 |
| Heart wall | 1.22 | 0.16 | 1.24 | 0.98 | 1.37 |
| Kidneys | 1.27 | 0.28 | 1.18 | 0.98 | 1.64 |
| Liver | 1.75 | 0.21 | 1.73 | 1.54 | 2.13 |
| Lungs | 1.07 | 0.15 | 1.07 | 0.84 | 1.25 |
| Muscle | 0.34 | 0.08 | 0.35 | 0.19 | 0.44 |
| Ovaries | 0.38 | 0.10 | 0.38 | 0.20 | 0.50 |
| Pancreas | 0.62 | 0.16 | 0.66 | 0.30 | 0.77 |
| Red marrow | 0.48 | 0.09 | 0.50 | 0.34 | 0.60 |
| Osteogenic cells | 0.55 | 0.09 | 0.54 | 0.44 | 0.71 |
| Skin | 0.24 | 0.05 | 0.24 | 0.14 | 0.31 |
| Spleen | 1.04 | 0.16 | 1.01 | 0.87 | 1.26 |
| Thymus | 0.46 | 0.12 | 0.48 | 0.23 | 0.58 |
| Thyroid | 0.29 | 0.07 | 0.29 | 0.17 | 0.38 |
| Urinary bladder wall | 0.27 | 0.06 | 0.27 | 0.17 | 0.36 |
| Uterus | 0.37 | 0.10 | 0.37 | 0.19 | 0.49 |
| Total body | 0.40 | 0.08 | 0.41 | 0.25 | 0.49 |
| Effective dose equivalent (mSv/MBq) | 0.72 | 0.09 | 0.73 | 0.56 | 0.83 |
| Effective dose (mSv/MBq) | 0.54 | 0.07 | 0.56 | 0.41 | 0.62 |
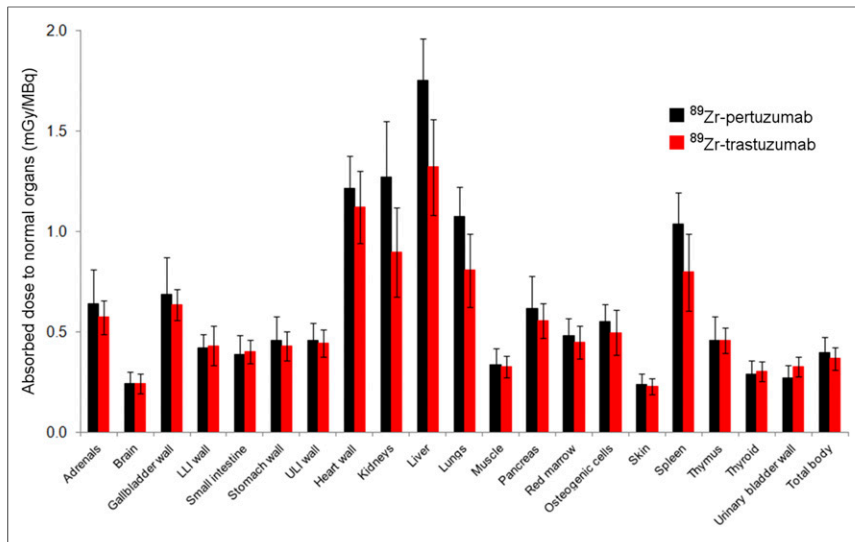
**FIGURE 2.** Comparative distributions of absorbed doses for $^{89}$Zr-pertuzumab and $^{89}$Zr-trastuzumab (16). Error bars denote SD. LLI = lower large intestinal; ULI = upper large intestinal.

therapy, including ado-trastuzumab emtansine in 2015, and was on trastuzumab therapy at the time of $^{89}$Zr-pertuzumab PET/CT. She had a recent diagnosis of brain metastases. $^{89}$Zr-pertuzumab PET/CT demonstrated a progressive increase in $^{89}$Zr-pertuzumab avidity over PET/CT scans obtained on days 1, 2, 6, and 8 after tracer administration (the SUV$_{max}$ of the most avid lesion was 13.6, 16.6, 26.0, and 30.1 on these 4 d) (Figs. 3A–3D). Blood-pool activity, including activity in the superior sagittal sinus, showed a continuing decrease over the scans. This feature allowed the most optimal visualization of the known brain metastases (Fig. 3E) on the day 8 scan (Fig. 3F).

Patient 2 had a left breast ER-positive, PR-positive, and HER2-positive (HER2 IHC 2+; HER2 amplification of 4.0 on FISH) IDC diagnosed in 2014. She had received HER2-directed therapy, including ado-trastuzumab emtansine in 2015–2016, and was on trastuzumab and pertuzumab therapy at the time of $^{89}$Zr-pertuzumab PET/CT. She had known supraclavicular nodal metastases at the time of $^{89}$Zr-pertuzumab PET/CT. There was relatively stable $^{89}$Zr-pertuzumab avidity on days 1, 2, 5, and 7 after tracer administration (the SUV$_{max}$ of the most avid lesion was 6.0, 4.7, 4.6, and 5.1 on these 4 d).

Patient 3 had a left breast ER-positive, PR-positive, and HER3-positive (HER2 IHC 3+) IDC that was diagnosed in 2014 and that was metastatic to the lung at the time of diagnosis. She had received HER2-directed therapy, including trastuzumab and pertuzumab, which she was receiving at the time of $^{89}$Zr-pertuzumab PET/CT. She had demonstrable $^{18}$F-FDG–avid disease in the left breast and left axillary nodes at the time of $^{89}$Zr-pertuzumab PET/CT. There was mildly increasing $^{89}$Zr-pertuzumab avidity on days 1, 2, 6, and 7 after tracer administration (the SUV$_{max}$ of the breast lesion was 3.7, 4.7, 6.3, and 5.5). Decreasing background avidity made the avid lesions most visible on the day 6 and 7 scans (Fig. 4). $^{89}$Zr-pertuzumab avidity was similar to $^{18}$F-FDG avidity (SUV$_{max}$, 6.6), which was obtained 3 wk earlier.

Patient 4 was diagnosed with ER-positive, HER2-negative (HER2 IHC 1+) IDC in 2003. At the time of $^{89}$Zr-pertuzumab PET/CT, she had demonstrable disease in the liver, bone, and chest wall on CT and MRI. She had previously received HER2-directed therapy, including trastuzumab and pertuzumab, which she was

receiving at the time of $^{89}$Zr-pertuzumab PET/CT. A recent biopsy of a right chest wall mass was HER2-positive (HER2 IHC 2+; HER2 amplification of 2.4 on FISH). There was low-level avidity in the right chest wall lesion (the SUV$_{max}$ was 2.8, 2.3, 2.4, and 2.4 on days 1, 4, 5, and 8 after $^{89}$Zr-pertuzumab administration, respectively).

Patient 5 was diagnosed with 2 distinct right breast malignancies in 2014: an ER-negative, HER2-positive (HER2 IHC 3+) malignancy and an ER-positive, HER2-negative (HER2 IHC 0) malignancy. She had previously received HER2-directed therapy, including trastuzumab and pertuzumab, which she was receiving at the time of $^{89}$Zr-pertuzumab PET/CT. She had demonstrable disease in the brain, lung, nodes, and liver at the time of $^{89}$Zr-pertuzumab PET/CT. Mild $^{89}$Zr-pertuzumab avidity in the brain, lung, and nodal lesions was greatest in the brain (the SUV$_{max}$ of the most avid brain lesion was 2.9, 6.1, and 6.1 on days 1, 2, and 5 after tracer administration, respectively). A brain metastasis was resected and was HER2-positive (IHC 2+; HER2 amplification of 2.4 on FISH); these findings confirmed that this site of $^{89}$Zr-pertuzumab-avidity was true-positive for a HER2-positive malignancy. Liver lesions did not show appreciable $^{89}$Zr-pertuzumab avidity above the liver background.

Patient 6 had a right breast ER-negative, HER2-positive (HER2 IHC 3+) IDC diagnosed in 2008. She had previously received HER2-directed therapy, including trastuzumab and pertuzumab, and was on ado-trastuzumab emtansine therapy at the time of $^{89}$Zr-pertuzumab PET/CT. She had only a small volume disease in thoracic and abdominal nodes at the time of $^{89}$Zr-pertuzumab PET/CT. Avidity in small nodes (the greatest being $1.5 \times 1.2$ cm in the right common iliac chain) was difficult to appreciate on $^{89}$Zr-pertuzumab PET/CT.

## DISCUSSION

In this first-in-human trial, we demonstrated safety and dosimetry for intravenously administered $^{89}$Zr-pertuzumab, which has been reviewed and accepted by the U.S. Food and Drug Administration. We also demonstrated successful HER2-targeted imaging in patients with HER2-positive metastatic breast cancer.

The mean effective dose of $^{89}$Zr-pertuzumab was 0.54 mSv/MBq, which is comparable to those of other radiolabeled antibody PET tracers, such as $^{89}$Zr-J591 (0.38 mSv/MBq) (16). In particular, the biodistribution and normal tissue dosimetry of $^{89}$Zr-pertuzumab are comparable to those of $^{89}$Zr-trastuzumab (0.48 mSv/MBq) (17). However, $^{89}$Zr-pertuzumab does appear to have slightly higher uptake in the central parenchymal organs (liver, kidney, spleen, and lung) than $^{89}$Zr-trastuzumab; this finding translates into a higher dose (mGy/MBq) by an average factor of approximately 1.3 for these organs. Because of their relatively slow kinetics, antibody-based PET tracers require radionuclides with relatively long physical half-lives. This requirement leads to radiation doses that are higher than those of small-molecule imaging agents that have fast kinetics and can use radionuclides with relatively short physical half-lives—the classic example being $^{18}$F-FDG.
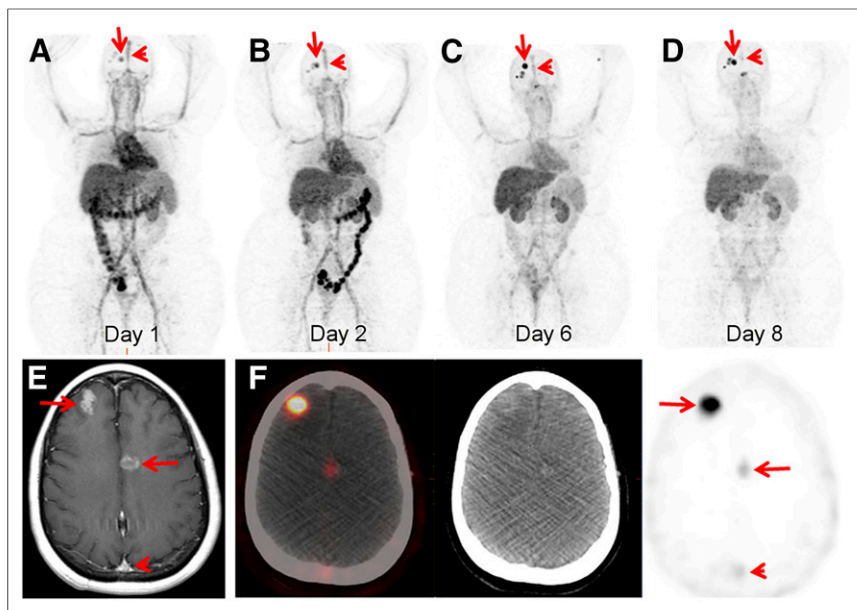
**FIGURE 3.** 46-y-old woman with both HER2-positive and HER2-negative primary breast malignancies and recently diagnosed brain metastases. Sequential maximum-intensity-projection images 1 d (A), 2 d (B), 6 d (C), and 8 d (D) after administration of $^{89}$Zr-pertuzumab. Blood-pool and liver background cleared on sequential images. Activity excreted by bowel was seen on days 1 and 2. Bilateral kidney activity was visualized on all days. Increasing activity in foci overlying skull was seen as time progressed (arrows). Decreasing activity was seen in blood pool of superior sagittal sinus (arrowheads). (E) Gadolinium-enhanced T1-weighed MR image of brain demonstrated enhancing brain metastases (arrows) and superior sagittal sinus (arrowhead). (F) Axial fused PET/CT, CT, and PET images 8 d after $^{89}$Zr-pertuzumab administration demonstrated avidity in brain metastases (arrows) and minimal residual avidity in superior sagittal sinus (arrowhead).

In the present study, we used a $^{89}$Zr activity ($\sim$74 MBq) that was lower than what we used in previous studies ($\sim$185 MBq). This activity was found to be adequate in terms of image quality for clinically feasible emission times, ranging from 4–8 min/bed position. As the radiation dose is directly proportional to the administered activity, this approach provided a significant reduction in the actual dose (mGy) compared with the doses used in our previous studies. Further, several investigators (20,21), including equipment manufacturers, are developing new, advanced methods of image reconstruction that should result in further significant reductions in radiation doses. The radiation exposures generated by radiolabeled antibody PET tracers would be justified if they produced clinically valuable information.

Imaging of $^{89}$Zr-pertuzumab was best performed 5–8 d after tracer administration. Scans on earlier days had higher liver and blood-pool backgrounds and tended to have lower tumor uptake. The combination of higher tumor uptake and lower backgrounds for imaging performed 5–8 d after tracer administration has been observed with other antibody tracers (16,17). The multiple-day delay in blood-pool clearance of antibody tracers can be considered a limitation of this technology. Potential alternatives include Affibody (Affibody AB) molecules (22) and single-domain antibodies (23,24), which have a rapid biodistribution, allowing for imaging within hours of tracer administration. Affibody molecules and single-domain antibodies labeled with tracers with shorter half-lives may have the added advantage of lower radiation doses to patients.

Although limited activity was seen in the bowel, we anticipate that this was the primary route for any $^{89}$Zr-pertuzumab excretion that did occur. Little measurable change was observed in whole-body activity after the first void (98% $\pm$ 1.8% of the prevoid measurement), and there was no visualization of activity in the urinary bladder at any time.

One potential clinical application of $^{89}$Zr-pertuzumab PET/CT is assessment of the HER2 status of disease—information that may not be accessible by biopsy (e.g., brain metastases). This application becomes increasingly important given the recent finding that in patients who have HER2-negative primary breast cancer and develop brain metastases, 20% will acquire HER2-positive metastases (7). Thus, a method of noninvasive, whole-body screening for HER2-positive disease would be of clinical value as a predictive biomarker (25), aiding in the selection of patients for HER2-targeted therapy on the basis of imaging. In this small trial, patients 1 and 5 had both HER2-positive and HER2-negative primary breast cancers and brain metastases. $^{89}$Zr-pertuzumab PET/CT imaging suggested that the brain metastases were HER2-positive; histologic proof was available in 1 of these patients.

Another potential clinical application of $^{89}$Zr-pertuzumab PET/CT is the assessment of HER2 heterogeneity. Patient 4 had a biopsy-proven HER2-negative primary breast malignancy but a biopsy-proven HER2-positive chest wall metastasis. Two previous liver biopsies for this patient were HER2-negative. The only site of
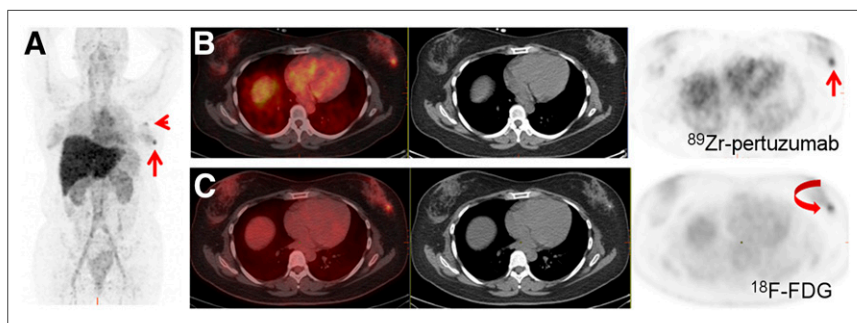


**FIGURE 4.** 58-y-old woman with HER2-positive breast cancer and current left breast and left axillary nodal disease. (A) Maximum-intensity-projection image 6 d after administration of $^{89}$Zr-pertuzumab demonstrated $^{89}$Zr-pertuzumab–avid left breast (arrow) and left axillary nodal (arrowhead) disease. (B) Axial fused PET/CT, CT, and PET images obtained 6 d after $^{89}$Zr-pertuzumab administration localized $^{89}$Zr-pertuzumab avidity in left breast (arrow). (C) Axial fused PET/CT, CT, and PET images from $^{18}$F-FDG PET/CT scan 3 wk earlier demonstrated corresponding $^{18}$F-FDG–avid breast lesion (arrow).

89Zr-pertuzumab avidity was the chest wall lesion, which was the only site of known HER2-positive disease, as defined by American Society of Clinical Oncology criteria. Of course, histologic analysis was not available for all sites of malignancy, but this early work suggests that [89]Zr-pertuzumab could be used to assess a heterogeneous HER2 tumor burden.

For this first-in-human pilot study of [89]Zr-pertuzumab PET/CT, the sample size of only 6 patients was primarily designed to provide normal tissue biodistribution and dosimetry data. Further information on the biodistribution of [89]Zr-pertuzumab in normal and malignant tissues will be generated in additional HER2-targeted imaging trials with this novel agent. Patients included in this trial had metastases that were treated with systemic therapy, often including HER2-targeted therapy, before trial enrollment. This scenario introduces difficulties in comparing the extents of active malignancies with radiotracer uptake. A treated HER2-positive metastasis may not have sufficient residual active tumor for visualization on PET. Despite this limitation, sites of disease that were avid for [89]Zr-pertuzumab were demonstrated in 5 of 6 patients. [89]Zr-pertuzumab–avid lesions were still demonstrated in patients who had previously received and were currently receiving HER2-targeted therapy. The effects of HER2-targeted therapy on [89]Zr-pertuzumab are not known; however, it was clear that HER2-targeted therapy did not prevent HER2-targeted imaging with [89]Zr-pertuzumab.

## CONCLUSION

This first-in-human trial demonstrated that [89]Zr-pertuzumab PET/CT may be safely performed and that [89]Zr-pertuzumab has the potential to be a clinically valuable HER2-targeted imaging agent for patients with metastatic breast cancer. Potential clinical applications include assessment of the HER2 status of lesions—information that may not be accessible by biopsy—and the assessment of HER2 heterogeneity. [89]Zr-pertuzumab PET/CT will next be used in a prospective clinical trial of patients with HER2-negative primary breast cancer to analyze the ability of [89]Zr-pertuzumab to detect unsuspected HER2-positive metastatic disease and help direct HER2-targeted therapy to appropriate patients.

## DISCLOSURE

## REFERENCES

1. Slamon DJ, Clark GM, Wong SG, Levin WJ, Ullrich A, McGuire WL. Human breast cancer: correlation of relapse and survival with amplification of the HER-2/neu oncogene. *Science*. 1987;235:177–182.
2. Slamon DJ, Leyland-Jones B, Shak S, et al. Use of chemotherapy plus a monoclonal antibody against HER2 for metastatic breast cancer that overexpresses HER2. *N Engl J Med*. 2001;344:783–792.
3. Romond EH, Perez EA, Bryant J, et al. Trastuzumab plus adjuvant chemotherapy for operable HER2-positive breast cancer. *N Engl J Med*. 2005;353:1673–1684.
4. Henry KE, Ulaner GA, Lewis JS. Human epidermal growth factor receptor 2-targeted PET/SPECT imaging of breast cancer: noninvasive measurement of a biomarker integral to tumor treatment and prognosis. *PET Clin*. 2017;12:269–288.
5. Ulaner GA, Hyman DM, Ross DS, et al. Detection of HER2-positive metastases in patients with HER2-negative primary breast cancer using [89]Zr-trastuzumab PET/CT. *J Nucl Med*. 2016;57:1523–1528.
6. Ulaner GA, Hyman DM, Lyashchenko SK, Lewis JS, Carrasquillo JA. [89]Zr-trastuzumab PET/CT for detection of human epidermal growth factor receptor 2–positive metastases in patients with human epidermal growth factor receptor 2–negative primary breast cancer. *Clin Nucl Med*. 2017;42:912–917.
7. Priedigkeit N, Hartmaier RJ, Chen Y, et al. Intrinsic subtype switching and acquired ERBB2/HER2 amplifications and mutations in breast cancer brain metastases. *JAMA Oncol*. 2017;3:666–671.
8. Hudis CA. Trastuzumab: mechanism of action and use in clinical practice. *N Engl J Med*. 2007;357:39–51.
9. Marquez BV, Ikotun OF, Zheleznyak A, et al. Evaluation of [89]Zr-pertuzumab in breast cancer xenografts. *Mol Pharm*. 2014;11:3988–3995.
10. Wolff AC, Hammond ME, Hicks DG, et al. Recommendations for human epidermal growth factor receptor 2 testing in breast cancer: American Society of Clinical Oncology/College of American Pathologists clinical practice guideline update. *J Clin Oncol*. 2013;31:3997–4013.
11. Oken M, Creech R, Tormey D, et al. Toxicity and response criteria of the Eastern Cooperative Oncology Group. *Am J Clin Oncol*. 1982;5:649–655.
12. Vosjan MJ, Perk LR, Visser GW, et al. Conjugation and radiolabeling of monoclonal antibodies with zirconium-89 for PET imaging using the bifunctional chelate *p*-isothiocyanatobenzyl-desferrioxamine. *Nat Protoc*. 2010;5:739–743.
13. Holland JP, Sheh Y, Lewis JS. Standardized methods for the production of high specific-activity zirconium-89. *Nucl Med Biol*. 2009;36:729–739.
14. Deri MA, Zeglis BM, Francesconi LC, Lewis JS. PET imaging with [89]Zr: from radiochemistry to the clinic. *Nucl Med Biol*. 2013;40:3–14.
15. Barrett PH, Bell BM, Cobelli C, et al. SAAM II: simulation, analysis, and modeling software for tracer and pharmacokinetic studies. *Metabolism*. 1998;47:484–492.
16. Pandit-Taskar N, O'Donoghue JA, Beylergil V, et al. [89]Zr-huJ591 immuno-PET imaging in patients with advanced metastatic prostate cancer. *Eur J Nucl Med Mol Imaging*. 2014;41:2093–2105.
17. O'Donoghue JA, Lewis JS, Pandit-Taskar N, et al. Pharmacokinetics, biodistribution, and radiation dosimetry for [89]Zr-trastuzumab in patients with esophagogastric cancer. *J Nucl Med*. 2018;59:161–166.
18. Sgouros G, Stabin M, Erdi Y, et al. Red marrow dosimetry for radiolabeled antibodies that bind to marrow, bone, or blood components. *Med Phys*. 2000;27:2150–2164.
19. Stabin MG, Sparks RB, Crowe E. OLINDA/EXM: the second-generation personal computer software for internal dose assessment in nuclear medicine. *J Nucl Med*. 2005;46:1023–1027.
20. Mikhaylova E, Tabacchini V, Borghi G, et al. Optimization of an ultralow-dose high-resolution pediatric PET scanner design based on monolithic scintillators with dual-sided digital SiPM readout: a simulation study. *Phys Med Biol*. 2017 Oct 19;62:8402–8418.
21. Behr SC, Bahroos E, Hawkins RA, et al. Quantitative and visual assessments toward potential sub-mSv or ultrafast FDG PET using high-sensitivity TOF PET in PET/MRI. *Mol Imaging Biol*. November 30, 2017 [Epub ahead of print].
22. Sörensen J, Sandberg D, Sandstrom M, et al. First-in-human molecular imaging of HER2 expression in breast cancer metastases using the ^{111}In-ABY-025 Affibody molecule. *J Nucl Med*. 2014;55:730–735.
23. Keyaerts M, Xavier C, Heemskerk J, et al. Phase I study of ^{68}Ga-HER2-Nanobody for PET/CT assessment of HER2 expression in breast carcinoma. *J Nucl Med*. 2016;57:27–33.
24. Xavier C, Vaneycken I, D'huyvetter M, et al. Synthesis, preclinical validation, dosimetry, and toxicity of ^{68}Ga-NOTA-anti-HER2 Nanobodies for iPET imaging of HER2 receptor expression in cancer. *J Nucl Med*. 2013;54:776–784.
25. Ulaner GA, Riedl CC, Dickler MN, Jhaveri K, Pandit-Taskar N, Weber W. Molecular imaging of biomarkers in breast cancer. *J Nucl Med*. 2016;57(suppl 1):53S–59S.